Monthly Notices
of the
ROYAL ASTRONOMICAL SOCIETY

MNRAS **441,** 3075–3082 (2014) doi:10.1093/mnras/stu751

Multicolour time series photometry of the variable star 1SWASP J234401.81−212229.1

C. Koen★

Department of Statistics, University of the Western Cape, Private Bag X17, Bellville, 7535 Cape, South Africa

Accepted 2014 April 11. Received 2014 April 7; in original form 2014 January 16

ABSTRACT

1SWASP J234401.81-212229.1 may be one of a handful of contact binaries comprising two M dwarfs. Modelling of the available observations is complicated by the fact that the radiation of the eclipsing system is dominated by a third star, a K dwarf. New photometry, presented in this paper, strengthens this interpretation of the data. The existence of such systems will have implications for the statistical distributions of masses in hierarchical multiple star systems.

Key words: binaries: close – stars: individual: 1SWASP J234401.81−212229.1.

1 INTRODUCTION

Recent explanations for the existence of a period minimum in W UMa contact binary stars have been published by Jiang et al. (2012) and Stępień & Gazeas (2012), where references to earlier work can be found. The models of Stępień & Gazeas (2012), in particular, predict a minimum period close to 0.20 d.

Observationally, very few confirmed contact systems with periods below 0.25 d have been found. Stępień & Gazeas (2012) list five such binaries, of which two have periods below 0.23 d, namely CC Com ($P = 0.2207$ d; Wenzel 1967) and GSC 01387-00475 ($P = 0.2178$ d; Rucinski & Pribulla 2008).

Large photometric surveys have found many new eclipsing binaries with very short periods and light-curve shapes suggestive of contact configurations. Becker et al. (2011) discovered 28 such stars, the majority with periods very close to 0.22 d. Two systems were found to have periods below 0.2 d: of these, SDSS J001641.03−000925.2 with $P = 0.1986$ d, has been confirmed as a contact binary by Davenport et al. (2013). The period of the other, SDSS J200011.19+003806.5, is only 0.1455 d. Nefs et al. (2013) announced the discovery of 14 binaries with periods below 0.23 d, and light curves indicative of contact systems. With one exception ($P = 0.1512$ d) periods were in the range 0.20–0.23 d. A directed search by Norton et al. (2011) of SuperWASP (Pollacco et al. 2006) time series photometry of thousands of stars for short-period eclipsing binaries produced 40 candidate contact systems with periods in the range 0.175–0.23 d. Lohr et al. (2014) confirmed one of these, 1SWASP J160156.04+202821.6, with $P = 0.2265$ d, as a W UMa binary.

The short-period ($P = 0.2137$ d) eclipsing system 1SWASP J234401.81−212229.1 (hereafter SWASP 2344) is unusual in that the single-lined K-type spectrum shows no detectable radial velocity variations. Furthermore, the star exhibits very large changes in its period. Lohr et al. (2013) discussed possible explanations, and concluded that the most likely is that almost all the light in the system is contributed by a relatively bright K5V star, hiding a much fainter contact binary system which is responsible for the eclipses. The apparent changes in the binary period are then due to a light time effect, as the close binary orbits the K star with a period of about 4.2 yr.

Given the discussion of short-period W UMa stars above, the star is clearly of some interest. This paper provides further evidence for the Lohr et al. (2013) hypothesis, based on 41 h of multicolour photometry of the star, obtained during six nights spanning a week.

2 THE OBSERVATIONS

All measurements were made with the SAAO (South African Astronomical Observatory) STE4 CCD camera mounted on the SAAO 1.0-m telescope at Sutherland, South Africa. The field of view of the camera on the telescope is 5×5 arcmin^2. Pre-binning of the images was performed throughout, giving a reasonable read-out time of about 17 s. Observations were cycled through various combinations of the *UBVRI* filterset – see Table 1 for an observing log. (Note that the *R* and *I* filters are R_C and I_C – but the subscripts are omitted for convenience). All of the observing was done under bright moonlight conditions, mostly through thin cirrus.

Photometric reductions were performed using an automated version of DOPHOT (Schechter, Mateo & Saha 1993). With few exceptions magnitudes determined from aperture photometry were preferred over profile-fitted magnitudes, since the latter were prone to trends with changing airmass. The analysis reported below was performed on differential magnitudes of SWASP 2344 primarily with respect to the relatively bright star 2MASS J23435106−2118405 ($I = 11.5$–Epchtein et al. 1999; hereafter the star is referred to as 2M 2343−2118). Comparison with several fainter stars in the field of view showed that the bright local standard is not overtly variable: on the few occasions when more than one comparison star was used,

★ E-mail: ckoen@uwc.ac.za

Table 1. The observing log. The range in the number of useful measurements (across different filters) is in the last column. Observations in *B* and *U* had to be abandoned halfway through the third and fifth runs, respectively, due to deteriorating weather conditions.

Starting time (HJD 245 6500+)	Filters	Run length (h)	*N*
79.2829	*UBVR*	6.6	58–61
80.2484	*UBVR*	7.3	71–80
82.2384	*BVR*	7.4	51–258
83.2490	*BVRI*	6.0	100–103
84.2431	*UVI*	6.4	61–121
85.5414	*UB*	7.4	92–101

the standard deviation of the 2M 2343−2118 measurements could be calculated, and was found to be in the range 4–18 mmag. Furthermore, the differences in the mean nightly magnitudes of stars should be almost constant if there is no variability on time-scales of days. Let $m_0(k)$ be the mean magnitude over night k of 2M 2343−2118, and $m_1(k)$ be the mean for a 'check' star. The range

$$r = \max_k(|m_0(k) - m_1(k)|) - \min_k(|m_0(k) - m_1(k)|)$$

is clearly a good measure of the constancy of both stars. Values of r were 38, 24, 18, 13 and 3 mmag for *UBVRI*, using a star which is 3.1 mag fainter than 2M 2343−2118 in *U*, and 1.85 mag fainter in *I*. Given that it is so much fainter, the check star may well be the primary contributor to the statistic r. Mean magnitudes of 2M 2343−2118 were therefore also used to set nightly zero-points.

As a final test of the suitability of 2M 2343−2118 as a local standard, 611 All Sky Automated Survey (Pojmanski 1997) photometric measurements of the star, spread over 9 years, were analysed. Over the frequency range 0–30 d^{-1} the highest peak in an amplitude spectrum was found to be 17 mmag, unremarkable compared to spectrum as a whole. The standard deviation of the measurements was only 57 mmag.

Light curves of SWASP 2344 are plotted in Figs 1–5 (Figs 2–5 online only). The shapes are typically those of a contact binary (e.g. Hilditch 2001, Kallrath & Milone 2009): continuous variability, with only slight differences in eclipse minima. Also shown are least-square fits based on the frequency 4.68 d^{-1} (Lohr et al. 2013), and several of its harmonics (see Table 2). In the case of the *U*-band data, an additional term in the subharmonic frequency is required in order to obtain a good fit: this appears to be a consequence of the noticeable difference between successive maxima in this filter (the O'Connell effect, see e.g. Hilditch 2001; Kallrath & Milone 2009). The effect is small, and will be ignored in the modelling of the light curves in Section 3.

Inspection of Table 2 shows a systematic increase with increasing wavelength of the amplitude of the principal term ($f = 9.36\,d^{-1}$). The same holds for the two other most prominent frequencies (4.68 and 18.72 d^{-1}): the one exception is the relatively small amplitude of the 4.68 d^{-1} frequency term in the *I* band.

The second part of the table demonstrates that there are no significant phase differences between the variations measured in the different filters, at least for those harmonics with sizeable amplitudes.

Table 3 has times of those minima, both primary and secondary, which are constrained by the data. The timings were found by locating the minima of the fitted curves (columns 2–6), and then

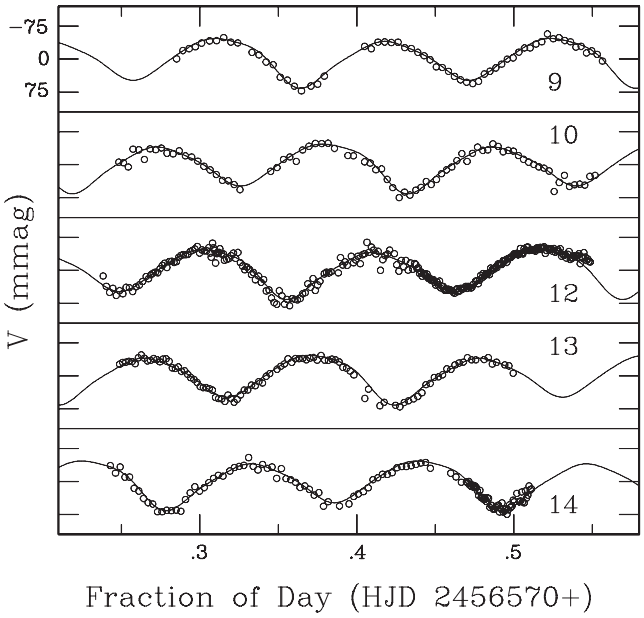

Figure 1. Light curves obtained in the *V* band. The height of each panel is 0.11 mag. Panels are labelled with the last two digits of the 'reduced' Julian Day of observation. The fitted curve was calculated from the values in Table 2.

averaging to obtain the final values (column 7). Epochs are determined from the ephemeris

$$T_n = T_0 + nP_0\,, \tag{1}$$

with $T_0 = 2454\,412.4743$ and $P = 0.213\,676$ d (Lohr et al. 2013). No attempt was made to estimate errors, as doing so would be complicated, and the results probably misleading (for example, uncertainties of the numbers in Table 3 are correlated). Comparison of the numbers in columns 2–6 suggest uncertainties of the order 0.001–0.002 d (roughly 1–3 min), though this is probably an underestimate of the true value.

3 THE CONTACT SYSTEM

In Fig. 6, the data in Figs 1–5 are shown phased with respect to the period of $P = 0.2137$ d. The fitted functions are of the form

$$y(\phi) = a_0 + \sum_{j=1}^{K}[a_j \cos(2\pi j\phi) + b_j \sin(2\pi j\phi)], \tag{2}$$

where $0 \le \phi \le 1$. For each filter, the value of K was determined by minimization of the Bayes Information Criterion (see Section 5 below); values for *UBVRI* were 2, 4, 6, 4 and 6 respectively. The phased data were 'cleaned' by iteratively removing points more than 3σ from the fitted curve. The final values of σ were 15.4, 8.5, 6.9, 7.5 and 6.4 mmag for *UBVRI*, respectively. The fitted curves can easily be used to calculate the phase dependence of colour indices, as demonstrated in Fig. 7. With the exception of $(V - I)$, colour changes are small.

Inspection of the Figs 6 and 7 reveals two pertinent facts: the amplitude of the variability *increases* with increasing wavelengths, and the system is bluest during eclipses. Both effects are explained by the Lohr et al. (2013) three-star theory: the variability is caused by a binary consisting of two cool M stars, while the hotter K-type

Table 2. A comparison of the amplitudes and phases obtained by least-squares fitting to the data of the known frequency of variation of SWASP 32344−2122, and its harmonics. Note that an additional subharmonic is required to fit the *U*-band data. Formal least-squares fitting errors are given in brackets.

Frequency (d^{-1})	Amplitudes (mmag)				
	U	*B*	*V*	*R*	*I*
2.340	9.8(1.2)				
4.680	4.7(1.2)	7.0(0.6)	6.7(0.5)	8.4(0.6)	4.6(0.6)
9.360	36.2(1.2)	40.0(0.6)	47.7(0.4)	54.3(0.6)	64.9(0.6)
14.040	2.2(1.2)	2.5(0.6)	3.0(0.5)	4.1(0.6)	1.8(0.6)
18.721	4.3(1.2)	4.7(0.6)	6.7(0.5)	10.3(0.6)	12.4(0.6)
23.400	1.4(1.2)	1.3(0.6)	2.1(0.4)	2.3(0.6)	2.0(0.6)
28.080	2.2(1.2)	2.1(0.6)	3.1(0.4)	3.1(0.6)	3.2(0.6)
Frequency (d^{-1})	Phases (rad)				
	U	*B*	*V*	*R*	*I*
2.340	−1.66(0.12)				
4.680	2.28(0.25)	3.08(0.09)	3.05(0.07)	2.99(0.07)	2.90(0.13)
9.360	1.37(0.03)	1.36(0.02)	1.42(0.01)	1.40(0.01)	1.42(0.01)
14.040	0.00(0.54)	−1.38(0.25)	−1.00(0.15)	−1.43(0.14)	−1.51(0.36)
18.721	2.59(0.28)	2.70(0.13)	2.94(0.07)	2.79(0.06)	2.92(0.05)
23.400	1.97(0.82)	0.10(0.49)	1.37(0.21)	0.48(0.25)	−0.02(0.30)
28.080	−1.65(0.53)	−1.88(0.29)	−1.35(0.15)	−1.61(0.19)	−1.95(0.19)

Table 3. The times of primary and secondary minima covered by the observations are given in columns 2–6, in the form of days after HJD 245 6570). Values were determined from the fitted curves in Figs 1–5. Averages are listed in the last column, and epochs determined from equation (1) are in column 1.

Epoch	Time of minimum					
	U	*B*	*V*	*R*	*I*	Mean
101 41	9.3652	9.3669	9.3641	9.3659		9.3655
101 41.5	9.4731	9.4718	9.4713	9.4711		9.4718
101 45.5	10.3278	10.3265	10.3259	10.3258		10.3265
101 46	10.4330	10.4353	10.4325	10.4343		10.4339
101 46.5	10.5426	10.5402	10.5397	10.5395		10.5405
101 54.5		12.2495	12.2491	12.2488		12.2491
101 55		12.3583	12.3556	12.3573		12.3571
101 55.5			12.4627		12.4625	12.4626
101 59.5		13.3179	13.3174	13.3171	13.3172	13.3174
101 60		13.4267	13.4240	13.4257	13.4255	13.4255
101 64	14.2792		14.2787		14.2801	14.2793
101 64.5	14.3887		14.3858		14.3856	14.3867
101 65			14.4924		14.4939	14.4932
101 68.5	15.2434	15.2410				15.2422
101 69	15.3480	15.3498				15.3489
101 69.5	15.4560	15.4546				15.4553

star contributes constant light. Since the relative contribution from the K star decreases with increasing wavelength, the variability is more obvious in red light, leading to the increased amplitude at longer wavelengths. Furthermore, the net contribution from the M dwarfs is less during eclipses, i.e. the bluer K star contributes more to the total radiation, and hence the system appears bluer.

The NIGHTFALL binary modelling package was used to explore fits to the data in Fig. 6. Without radial velocities the solutions are, of course, not well constrained. Table 4 shows three locally optimal models. Roche lobe filling factors were 1.2 in all three cases – increasing the value did not improve the fit noticeably, while smaller values led to notably suboptimal solutions.

It is noteworthy that the mass ratios, inclinations and third light contributions are very similar for the three models. Also note that Lohr et al. (2013) found $q = 0.5$, $i = 77^\circ$. The reduced χ^2 values are large, indicating that the fit is inadequate: for one, the O'Connell effect suggests that there may be spots on the surface, which would require more detailed modelling. Fitted light curves are plotted in Fig. 8.

The third light fractions in Table 4 can be used to estimate the colours of the overcontact system. Let

$$\alpha_j = F_{\rm K}(\lambda_j)/[F_{\rm K}(\lambda_j) + F_{\rm O}(\lambda_j)],$$

where $F_{\rm K}(\lambda_j)$ and $F_{\rm O}(\lambda_j)$ are the fluxes of the K star and the overcontact system, respectively, at wavelength λ_j. The corresponding magnitudes are $m_{\rm K}(\lambda_j)$ and $m_{\rm O}(\lambda_j)$. Also let

$$\beta_j = 1/\alpha_j - 1 \ = F_{\rm O}(\lambda_j)/F_{\rm K}(\lambda_j),$$

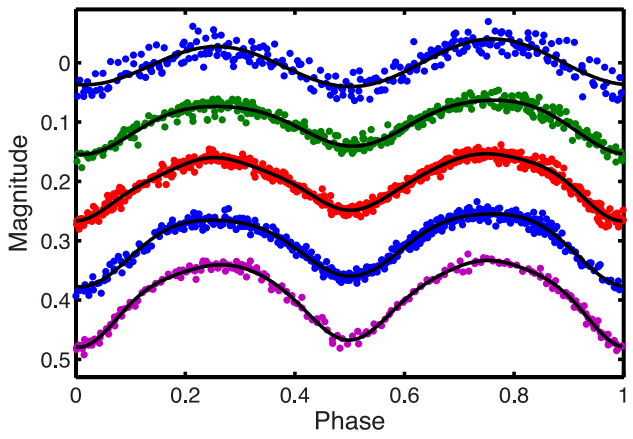

Figure 6. Measurements phased with respect to the 0.214 d period. From top to bottom are *U*, *B*, *V*, *R* and *I*. Also shown are least-squares fit of equation (2). The zero-point of the data for each filter is arbitrary. The increase of amplitude with increasing wavelength is noteworthy.

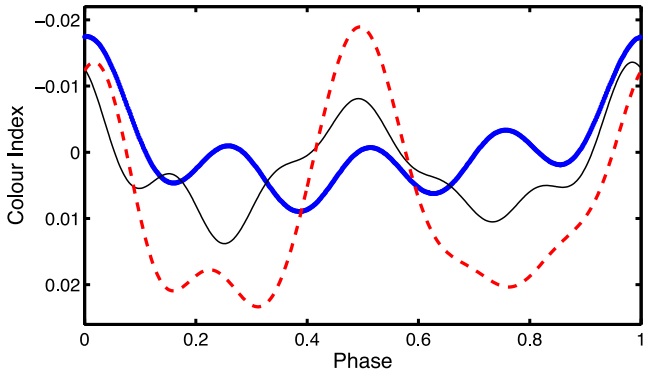

Figure 7. Colour indices calculated from the fitted curves in Fig. 6. Thick solid line: $(U-B)$; thin solid line: $(B-V)$; dashed line: $(V-I)$.

which results in $\beta = 0.23, 0.21, 0.21, 0.27, 0.34$ for *UBVRI*. It is straightforward to show that the colour indices of the overcontact system are

$$m_{\rm O}(\lambda_i) - m_{\rm O}(\lambda_j) = m_{\rm K}(\lambda_i) - m_{\rm K}(\lambda_j) - 2.5\log_{10}(\beta_i/\beta_j).$$

Using $(U-B) = 1.06$, $(B-V) = 1.15$, $(V-R) = 0.68$ and $(V-I) = 1.20$ for a K5V star (http://www.stsci.edu/~inr/intrins.html), the overcontact binary colours

$$(U-B) = 0.94 \quad (B-V) = 1.15 \quad (V-R) = 0.95$$

$$(V-I) = 1.74$$

Table 4. Three illustrative overcontact binary models fitted to the multi-colour photometry, using the NIGHTFALL package. The figures in column 5 are the fractions of the total system flux contributed by the K star. Further details are given in the text.

T_1 (K)	T_2 (K)	q	i (°)	Third light (*UBVRI*)	Reduced χ^2
3560	3480	2.16	77.3	0.810,0.828,0.829,0.791,0.744	1.581 03
3475	3395	2.33	78.6	0.811,0.828,0.828,0.790,0.745	1.568 32
3370	3305	2.37	79.4	0.814,0.828,0.827,0.791,0.746	1.563 89

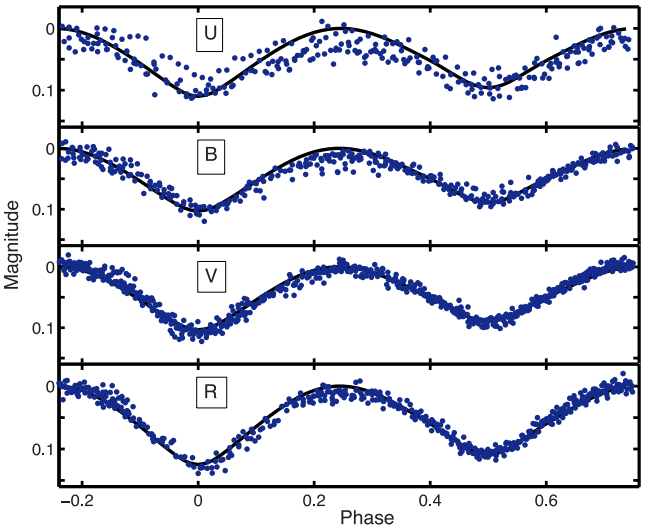

Figure 8. Model fits to the *UBVR* data in Fig. 6.

follow. Unfortunately, these indices do not correspond even remotely to any one spectral type: in particular, the $(U-B)$ index is far too blue for a regular M star. It is perhaps worth noting that the anomalously blue $(B-V)$ index of the very similar overcontact system GSC 2314−0530 was recently remarked on by Dimitrov & Kjurkchieva (2010). The authors point to this as a general feature of dMe stars.

4 TIME SERIES MODELLING OF THE COMBINED SWASP AND SAAO PHOTOMETRY

The top panel of Fig. 9 contains an amplitude spectrum of the combined new *V*-filter data and the SWASP observations; spectra of the combined *R*-filter and SWASP data, and of the SWASP data only, are very similar. The spectrum is dominated by the 46 mmag peak at $f_0 = 9.359\,944\,{\rm d}^{-1}$, and its alias pattern. Pre-whitening by the peak frequency leads to the spectrum in the lower panel. Alias patterns centred on the first and second harmonic frequencies 18.72 and 28.08 $\rm d^{-1}$ are obvious, as is the power excess at the subharmonic 4.68 $\rm d^{-1}$. Closer inspection shows some 'grass' in the

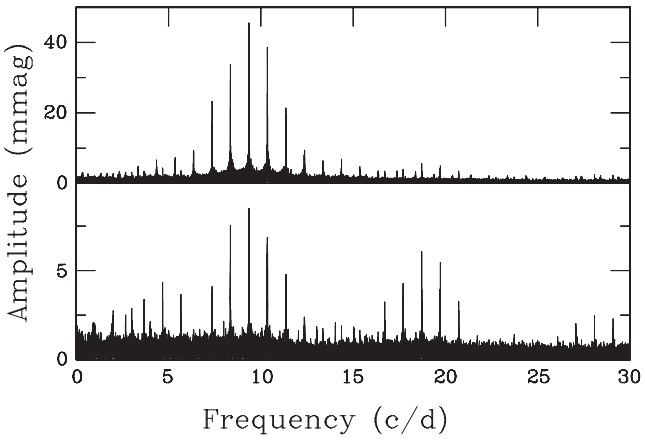

Figure 9. An amplitude spectrum of the combined SWASP, and SAAO *V*-filter data (top panel). The bottom panel shows the spectrum after pre-whitening of the data by a sinusoid with a frequency of $f_0 = 9.359\,944\,{\rm d}^{-1}$. Note that the residual spectrum is still largely dominated by features near 9.3 $\rm d^{-1}$, and its aliases.

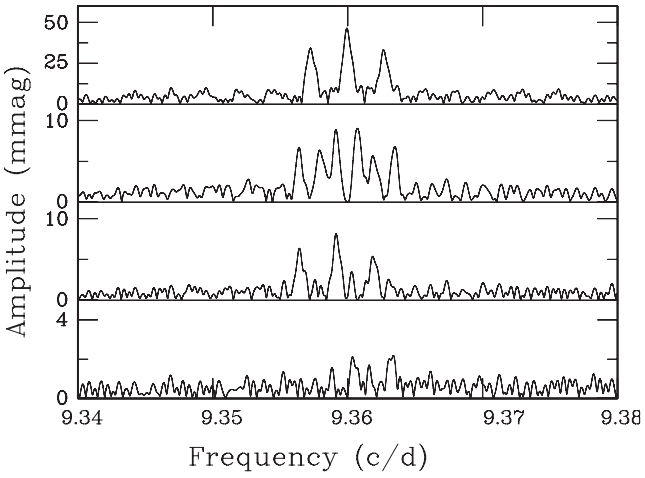

Figure 10. Successive pre-whitening of frequencies in a narrow range around f_0. The top panel shows peaks at f_0, and two aliases. Removal of f_0 shows that it is actually a blend of f_0 and two adjacent frequencies (second panel). Removal of all three frequencies leads to the residual spectrum in the bottom panel. Note the different vertical scales of the panels.

range 13–15 d^{-1}, which analysis reveals to be due to a power excess at $1.5 \times 9.36 = 14.04\,\mathrm{d}^{-1}$. At low frequencies, there are also peaks at multiples of $1\,\mathrm{d}^{-1}$, most likely due to small zero-point offsets of different sections of the data.

At $9.360\,725\,\mathrm{d}^{-1}$, the frequency of the main peak in the residual spectrum in the bottom panel of Fig. 9 is very close to the principal frequency in the top panel. Successive pre-whitening of frequencies in a narrow range around f_0 is explored in Fig. 10. The top panel shows peaks on either side of f_0, at a separation of $0.0027\,\mathrm{d}^{-1}$, corresponding to a period ∼370 d – evidently one cycle per year aliases. Pre-whitening of f_0 leads to the residual spectrum in the second panel: removal of f_0 has revealed that the spectrum peak in the top panel is actually a blend of three closely spaced frequencies, with the two side frequencies at separations Δf of 0.000 78 and $0.000\,80\,\mathrm{d}^{-1}$ from f_0. The amplitudes of these peaks are 9 and 8 mmag, respectively, and if they are pre-whitened from the data, the largest remaining peak in the spectrum (bottom panel of Fig. 7) is about 2 mmag in height.

Similar triplets, with similar separations, are found at the second and third harmonics of f_0. The subharmonic shows a single peak near $f_0/2$, while $1.5f_0$ has a weak doublet structure (amplitudes 2.1 and 1.4 mmag) with separation $0.001\,\mathrm{d}^{-1}$. For the triplets, separations are in the range $7.6-8.2 \times 10^{-4}\,\mathrm{d}^{-1}$.

Symmetrical triplets are obtained in spectra of data generated in accordance with

$$y(t) = B\cos\{2\pi f[t + \Delta T(t)] + \phi\} + \text{error}$$

$$\Delta T(t) = A\cos(2\pi t/P + \psi), \tag{3}$$

where A, B are amplitudes; ϕ, ψ are phase angles; and P is a modulation period. The frequency separation in the resultant triplet in the spectrum is $\Delta f = 1/P$. Modulation of the form (3) is exactly what results from a light time effect.

5 THE LIGHT TRAVEL-TIME EFFECT

The material in Section 4 is consistent with the Lohr et al. (2013) three-star system. In this model, the short-period eclipsing binary is in orbit around the K dwarf (more accurately: around the centre of mass), and the photon arrival times are modulated by a light time effect. The following model is therefore fitted to the observations:

$$y(t) = \sum_{j=1}^{5} B_j \cos\{2\pi f_j[t + \Delta T(t)] + \phi_j\} + \text{error}$$

$$\Delta T(t) = A\left\{\frac{1-e^2}{1+e\cos\theta(t)}\sin[\theta(t)+\omega] + e\sin\omega\right\}, \tag{4}$$

where e is the eccentricity and ω describes the orientation of the elliptical orbit, in the plane containing the orbit. The amplitude is

$$A = a\sin i/c, \tag{5}$$

where a is the length of the semimajor axis and i the orbital inclination angle. In keeping with the findings above, the light curve of the short-period binary is described by the set of five frequencies $\{f_0/2, f_0, 3f_0/2, 2f_0, 3f_0\}$. The true anomaly $\theta(t)$ is given by the solution of

$$E(t) - e\sin E(t) = \frac{2\pi}{P}(t - t_0)$$

$$\theta(t) = 2\arctan\left[\sqrt{\frac{1+e}{1-e}}\tan\frac{E(t)}{2}\right], \tag{6}$$

where P is the orbital period of the close eclipsing system around the third star, and t_0 is the time 'zero-point' (such that the eccentric anomaly $E(t_0) = 0$). A standard source for these equations is Irwin (1952).

Estimates of the quantities of primary interest, namely the binary period P and the modulation amplitude A, are plotted in Fig. 11 as functions of the eccentricity. Also shown are the corresponding mean squared errors (MSE). Results are displayed for both unweighted data, and for the case where the SAAO data are weighted

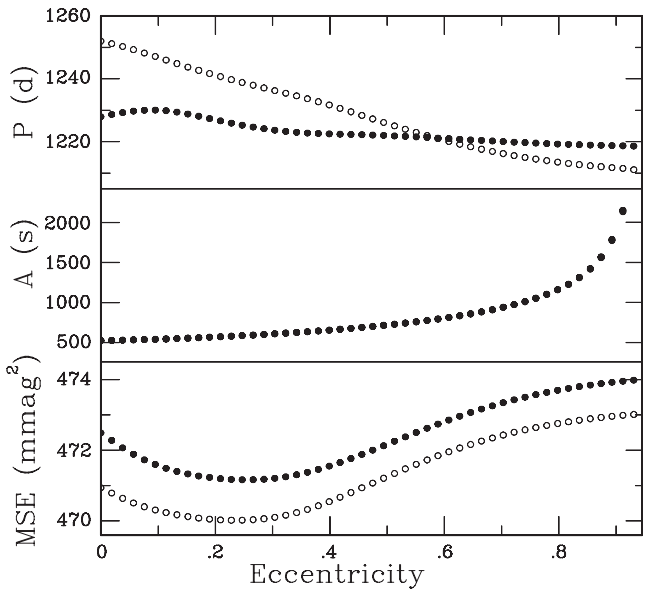

Figure 11. Estimated values of the orbital period of the contact system around the K star (top panel), and of the light time amplitude (middle panel). Open and filled circles show estimates based on unweighted and weighted data, respectively. Corresponding mean squared errors are in the bottom panel: the zero-point for the weighted data results is arbitrary. Values are shown as functions of the assumed eccentricity. These results are based on the combined SuperWASP and SAAO V-filter measurements.

by a factor 4.8 with respect to the SuperWASP data. (This figure was arrived at by comparing residual variances of the zero-eccentricity fit. The corresponding weight for the SAAO *R*-filter data is 2.97).

There is some slight evidence for a non-zero eccentricity, in that the MSE reaches a minimum near $e = 0.2$. Model information criteria can be used to evaluate whether the additional complexity of the model with $e \neq 0$ is merited by the small reduction in MSE, as compared to the model with $e = 0$. The Akaike and Bayes information criteria are respectively given by

$$\mathrm{AIC} = N \log(\mathrm{MSE}) + 2K$$

$$\mathrm{BIC} = N \log(\mathrm{MSE}) + K \log N, \quad (7)$$

where N is the number of data and K the number of model parameters (e.g. Burnham & Anderson 2002). Note that both the criteria are sums of two terms, the first of which measures model fit, and the second model complexity (in the sense of the number of model parameters). It is obviously desirable to minimize both terms in an information criterion, i.e. the model with the minimum information criterion is preferred. The two criteria in equation (7) differ in the way in which model complexity is weighted (more heavily in the BIC).

If $e = 0$, then equations (3)– (5) reduce to

$$\Delta T = A \sin[\theta(t) + \omega] = A \sin\left[\frac{2\pi}{P}(t - t_0) + \omega\right] \quad (8)$$

and ω can be absorbed into t_0. (Alternatively, for a circular orbit, ω is not defined.) The number of model parameters K in equation (7) is therefore two fewer for $e = 0$. The preferred model, according to both criteria, is that with e in the range 0.24–0.26, with the exact value depending on whether data have been weighted. Corresponding estimated parameter values are $P = 1225$–1240 d and $A = 582$–590 s. These values are not very dissimilar from $P = 1228$–1252 d and $A = 527$ s for the zero-eccentricity case.

Figs 12 and 13 (online only) show the corresponding results for the SuperWASP+*R* data, and the SuperWASP data only. Parameter estimates for the $e = 0$ and optimal $e \neq 0$ models are summarized in Table 5. Aside from the somewhat larger value of P derived from the SuperWASP-only data, there is reasonable agreement amongst the various data sets. Periods estimated from the larger data sets should probably be favoured, since the time baseline covered is longer by about 600 d. It is also noteworthy that the SuperWASP data set on its own does not support non-zero eccentricity, though this may also be due to its shorter baseline.

An amplitude spectrum of the residuals of the model (3) fit is featureless, aside from peaks at $1\,\mathrm{d}^{-1}$ and its aliases (as in the bottom panel of Fig. 9). These artefacts aside, the spectrum is that of noise at the ∼1 mmag level.

6 ORBITAL INCLINATION OF THE LONG-PERIOD SYSTEM

The values of P and A derived in the preceding section can be used to estimate the inclination (with respect to the plane of the sky) of the orbit of the eclipsing binary in the three-star system. Kepler's third law can be written in the form

$$a_1 + a_2 = 4.21 P^{2/3} (M_1 + M_2)^{1/3},$$

where a_1 and a_2 are the lengths of the semimajor axes of the orbits of the primary K5 star and the close pair (in $\mathrm{R}_\odot$); M_1 is the mass of the K5 star, and M_2 the total mass of the eclipsing system (in $\mathrm{M}_\odot$); and the period P is in days. Using

$$M_1 a_1 = M_2 a_2,$$

this can be rewritten as

$$a_2 = 4.21 P^{2/3} (M_1 + M_2)^{1/3} (1 + M_2/M_1)^{-1}\ .$$

It then follows from (5) that

$$\sin i = 0.10 \frac{A}{M_1} \left(\frac{M_1 + M_2}{P}\right)^{2/3}\ .$$

Assuming

$$M_1 = 0.7\,\mathrm{M}_\odot \qquad 0.5 \leq M_2 \leq 1\,\mathrm{M}_\odot \qquad 1225 \leq P \leq 1270\ \mathrm{d}$$

$$527 \leq A \leq 590\ \mathrm{s}$$

(Table 5), $46 \leq i \leq 90^\circ$ is obtained. Further time series observations will further constrain P and A, while careful modelling should help to narrow the limits on M_2. The difference between this inclination, and that of the inner binary ($i \approx 78^\circ$ – see Table 3) may have important dynamical consequences, as will be discussed below.

Table 5. Light-time models fitted to the SWASP data, with and without SAAO data. Data set size N is in the second column. For each data set the first line gives the zero-eccentricity model, and the second the optimal (as measured by the information criteria) model with non-zero eccentricity. For each model the information criteria are measured with respect to values at zero eccentricity. In the models with weighting, SAAO data received weights of 4.8 (V) or 2.97 (R) with respect to the SuperWASP observations.

Data set	N	Eccentricity e	Period P (d)	Amplitude A (s)	ΔAIC	ΔBIC
SWASP+V	22 174	0	1252	527	0	0
(No weighting)		0.24	1240	582	−33.1	−17.1
SWASP+V		0	1228	527	0	0
(Weighted)		0.26	1225	590	−48.6	−32.6
SWASP+R	220 40	0	1270	532	0	0
(No weighting)		0.22	1257	579	−27.9	−11.9
SWASP+R		0	1250	532	0	0
(Weighted)		0.24	1246	586	−41.5	−25.5
SWASP	215 40	0	1328	534	0	0
		0.13	1317	546	1.6	17.5

7 DISCUSSION

Until fairly recently very few binaries consisting of two M dwarfs were known. Dimitrov & Kjurkchieva (2010) listed 17 such systems. Of these, all but two were classified as detached; the two shortest period systems ($P = 0.192$ and 0.198 d, respectively) were thought to be semidetached. In other words, as of 2010, there were no confirmed contact binaries made up of two M dwarfs.

Since then the difficult task of finding such stars has been aided enormously by the advent of large-scale searches for e.g. planetary transits, which have led to the discovery of large numbers of variable stars of different types. Several efforts have been directed at finding eclipsing binaries with very short periods, and/or systems made up of two M stars, from observations gathered by such surveys (e.g. Becker et al. 2011; Coughlin et al. 2011; Hartman et al. 2011; Norton et al. 2011; Birkby et al. 2012; Nefs et al. 2013; Palaversa et al. 2013; Zendejas Dominguez et al. 2013). In most cases, the new photometric discoveries have not yet been followed up by spectroscopic classifications, radial velocity measurements or detailed modelling. For example, of the 53 candidate systems in table 1 of Norton et al. (2011), only three have published spectral types at the time of writing.

Only one system appears to have been confirmed as an overcontact binary consisting of two M dwarfs, namely SDSS J001641−000925 (Davenport et al. 2013). It has a period of 0.20 d, and the two components have masses of 0.54 and 0.34 $M_\odot$.

The importance of such systems for the understanding of binary star evolution has been argued by Nefs et al. (2013). Briefly, it is generally believed that the very short period contact systems evolved from longer period systems, on a time-scale which increases with decreasing mass. Inspection of fig. 3 in Nefs et al. (2013) suggests that for a primary star mass below 0.5 $M_\odot$, the progenitor binary period would have needed to be below 1.5 d, in order for SWASP 2344 to arrive at its present configuration in less than 12 Gyr. (There are a number of assumptions involved, such as small mass-loss, and orbital synchronization). However, this appears to be in conflict with observational evidence, since there is currently not a single known main-sequence binary in a young cluster with a period below 1.7 d, suggesting that such objects (if they exist) are extremely rare.

It seems likely that the K dwarf will have been little affected by the evolution of the close binary, hence detailed modelling of it may shed more light on the age of the system (e.g. Fernandes, Vaz & Vicente 2011).

On the other hand, it is possible that the K star has played a dynamical part in shortening the period of the M star binary. In particular, the non-alignment of the inner and outer orbits demonstrated in Section 6 can cause precession of the inner-binary orbital plane (e.g. Fabrycky & Tremaine 2007). Under certain conditions (see e.g. Kisseleva-Eggleton & Eggleton 2010) the inner-binary orbital eccentricity and inclination can even change cyclically, with a period of order $P_{\rm outer}^2/P_{\rm inner}$ ('Kozai oscillations'; Kozai 1962). Although the current orbital parameters of SWASP 2344 do not satisfy all the requirements for Kozai oscillations, this effect may have played a role in the earlier dynamical evolution of the system.

It is interesting to place SWASP 2344 in the context of 63 triple systems harbouring $P > 1$ d spectroscopic binaries, as described by Tokovinin et al. (2006). The three shortest outer-binary periods are 3.3, 4.1 and 4.3 yr, and a further four periods are shorter than 10 yr. The two largest ratios of tertiary component mass to close binary primary mass are 1.33 and 1.49. The corresponding numbers for SWASP 2344 are ∼3.6 yr for the outer binary period, and 0.67/0.4 ≈ 1.7 for the ratio of masses of a K5 and an M2 star (Schmidt-Kaler 1982).

The figures given in the preceding paragraph are, of course, quite uncertain. Nonetheless, the confirmation of SWASP 2344 as a triple system in which the wide component is clearly the more massive by some margin, points to a likely selection effect amongst known multiple systems. It may be surmised that there are many close hierarchical triples in which the light is dominated by the wide component, hence obscuring the multiplicity of the system. It may be necessary to qualify the statement that '... the most massive components in multiple systems are preferentially found in close subsystems' (Tokovinin et al. 2006).

ACKNOWLEDGEMENTS

The author is grateful to Marcus Lohr for graciously supplying the SuperWASP observations of SWASP 2344; to Dr Rainer Wichmann for the public availability of the NIGHTFALL software; and to those maintaining the Simbad data base in Strasbourg, France. Financial support from the South African National Research Foundation, and telescope time allocated by SAAO, are also gratefully acknowledged. The referee's comments led to improvements in the paper.

REFERENCES

Becker A. C., Bochanski J. J., Hawley S. L., Ivezić Ž, Kowalski A. F., Sesar B., West A. A., 2011, ApJ, 731, 17
Birkby J. et al., 2012, MNRAS, 426, 1507
Burnham K. P., Anderson D. R., 2002, Model Selection and Multimodel Inference: A Practical Information-Theoretic Approach, 2nd edn. Springer, New York
Coughlin J. L., López-Morales M., Harrison T. E., Ule N., Hoffman D. I., 2011, AJ, 141, 78
Davenport J. R. A. et al., 2013, ApJ, 764, 62
Dimitrov D. P., Kjurkchieva D. P., 2010, MNRAS, 406, 2559
Epchtein N. et al., 1999, A&A, 349, 236 (DENIS catalogue)
Fabrycky D., Tremaine S., 2007, ApJ, 669, 1298
Fernandes J. M., Vaz A. I. F., Vicente L. N., 2011, A&A, 532, A20
Hartman J. D., Bakos G. A., Noyes R. W., Sipőcz B., Kovács G., Mazeh T., Shporer A., Pál A., 2011, AJ, 141, 166
Hilditch R. W., 2001, An Introduction to Close Binary Stars. Cambridge Univ. Press, Cambridge
Irwin J. B., 1952, ApJ, 116, 211
Jiang D., Han Z., Ge H., Yang L., Li L., 2012, MNRAS, 421, 2769
Kallrath J., Milone E. F., 2009, Eclipsing Binary Stars: Modelling and Analysis, 2nd edn. Springer, New York
Kisseleva-Eggleton L., Eggleton P. P., 2010, in Prša A., Zejda M., eds, ASP Conf. Ser. Vol. 435, Binaries – Key to Comprehension of the Universe. Astron. Soc. Pac., San Francisco, p. 169
Kozai Y., 1962, AJ, 67, 591
Lohr M. E., Norton A. J., Kolb U. C., Boyd D. R. S., 2013, A&A, 558, A71
Lohr M. E., Hodgkin S. T., Norton A. J., Kolb U. C., 2014, A&A, 563, 34
Nefs S. V. et al., 2013, MNRAS, 431, 3240
Norton A. J. et al., 2011, A&A, 528, A90
Palaversa L. et al., 2013, ApJ, 146, 101
Pojmanski G., 1997, Acta Astron., 47, 467
Pollacco D. et al., 2006, PASP, 118, 1407
Rucinski S. M., Pribulla T., 2008, MNRAS, 388, 1831
Schechter P. L., Mateo M., Saha A., 1993, PASP, 105, 1342
Schmidt-Kaler T., 1982, in Schaifers K., Voigt H. H., eds, Landolt-Börnstein Series, Vol. 2b. Springer-Verlag, Berlin, p. 17
Stępień K., Gazeas K., 2012, Acta Astron., 65, 153
Tokovinin A., Thomas S., Sterzik M., Udry S., 2006, A&A, 450, 681
Wenzel W., 1967, Mitt. Verän. Sterne Sonneberg, 4, 60
Zendejas Dominguez J. et al., 2013, A&A, 560, A92

SUPPORTING INFORMATION

Additional Supporting Information may be found in the online version of this article:

Figure 2. As for Fig. 1, but for the *B* band.
Figure 3. As for Fig. 1, but for the *R* band.
Figure 4. As for Fig. 1, but for the *U* band.
Figure 5. As for Fig. 1, but for the *I* band.
Figure 12. As for Fig. 11, but for the combined SuperWASP, and SAAO *R* filter, data.
Figure 13. As for Fig. 11, but for the SuperWASP data only.
(http://mnras.oxfordjournals.org/lookup/suppl/doi:10.1093/mnras/stu751/-/DC1).

Please note: Oxford University Press is not responsible for the content or functionality of any supporting materials supplied by the authors. Any queries (other than missing material) should be directed to the corresponding author for the paper.

This paper has been typeset from a TEX/LATEX file prepared by the author.